Hall Thruster Plume Measurements of Time Resolved Ion Energy

IEPC-2019-516

Presented at the 36th International Electric Propulsion Conference
University of Vienna, Austria
September 15-20, 2019

Matthew J. Baird* Thomas V. Kerber† and Kristina M. Lemmer‡
Western Michigan University, Kalamazoo, MI, 49008, USA

and

Wensheng Huang§
National Aeronautics and Space Administration Glenn Research Center, Cleveland, OH, 44135, USA

High-speed retarding potential analyzer (RPA) measurements were made to determine the time-resolved ion energy distribution function in a 200 W Hall thruster. Multiple ion energy populations exist in Hall thruster discharge plumes. This diagnostic utilized a standard RPA design and DC to 1 MHz bandwidth collector current measurement at discrete energy filtration bias levels. A Fast Fourier Transform transfer function algorithm was used to temporally reconstruct the collector current over all energy filtration levels using simultaneously triggered thruster discharge current measurements. RPA collector spectral density profile showed a large dependence on the filtration bias level and complex low-energy populations were revealed.

*Ph.D. Student, Mechanical and Aerospace Engineering Department, 1903 W Michigan Avenue, MS 5343, matthew.j.baird@wmich.edu.
†Masters Student, Mechanical and Aerospace Engineering Department, 1903 W Michigan Avenue, MS 5343, thomas.v.kerber@wmich.edu.
‡Associate Professor, Mechanical and Aerospace Engineering Department, 1903 W Michigan Avenue, MS 5343, kristina.lemmer@wmich.edu.
§Propulsion Scientist, Electric Propulsion Systems, wensheng.huang@nasa.gov.

Nomenclature

A_{coll}	Collector current FFT complex coefficients
A_{disch},A^*_{disch}	Discharge current FFT complex coefficients, arbitrary coefficient set
d	characteristic RPA length, m
E_z	axial electric field component, V/m
$\Delta f, f_s$	Fast Fourier transform frequency resolution and sample frequency, Hz
I_{coll},$\bar{I}_{coll}$,I'_{coll},$I_{synthcoll}$	time varying, time averaged, AC reconstructed, and fully synthesized collector current, A
$I_{disch,i}$,I^*_{disch}	Hall thruster discharge current from the i-th V_{bias} and an arbitrary discharge current signal, A
H_{coll}	FFT transfer function
m	ion mass, kg
N	sample size
P_{disch}	Hall thruster discharge power, W
q	fundamental charge, 1.602E-19 C
v_0	initial ion velocity, m/s
V_{bias}	RPA discrimination grid potential, V
V_{disch}	Hall thruster discharge voltage, V
R	RPA radial distance, mm
z	RPA axial spatial dimension, mm
Δt	ion dwell time, s
ϵ	ion energy level, eV
θ	RPA angle with respect to thruster centerline, $^\circ$

I. Introduction

Hall effect thrusters (HET) are a subcategory of electric propulsion devices in which electrical energy is used to ionize and accelerate a propellant through the use of a carefully designed electromagnetic field. HETs are predominantly accompanied by a low work function hollow cathode to provide seed electrons for breakdown and beam neutrality. From their earliest development by the United States and Russia in the 1960's until present day, hundreds of HETs have flown on spacecraft serving research, military, and commercial needs while demonstrating excellent reliability.[1] NASA has plans to utilize HETs for both science and exploration missions, with upcoming flights on the Psyche Discovery mission and the Power and Propulsion Element of the NASA Gateway.[2,3,4,5,6]

Although HETs have had ample heritage, the dynamics within the plasma discharge are not fully understood. Thruster discharge oscillations may influence operating temperature, electron transport across magnetic field lines, and overall thruster stability.[7,8,9] Moreover, multiple ion energy populations exist in the HET plasma system. These ion energy populations can consist of thermal charge exchange (CEX) ions, accelerated beam ions, and high-energy ions formed at the cathode and accelerated to energies exceeding the cathode external electric fields.[10] Each ion energy population carries with it the potential for unique behavior that is difficult to study with time-averaged diagnostics. Many efforts have been performed to capture ion dynamics of HETs and cathodes in the past. These include Time-Resolved Laser Induced Florescence (TR-LIF), Silicon photomultiplier arrays (SiPM), double ion saturation probes, and high speed imaging.[11,12,7,8,9] As Hall thrusters are scaled to higher power levels and used for deep space missions, it becomes more important to understand the dynamic behavior of ions so that we may continue to operate with a high degree of confidence and develop predictive models that capture ion oscillations. This paper describes efforts towards the development of a novel diagnostic with the potential to reveal overall temporal ion energy behavior and the constituent ion energy population behavior.

II. Background

A. Retarding Potential Analyzer Diagnostic

A retarding potential analyzer (RPA) was used to discriminate and measure ion energy populations within the beam of a 4.4-cm diameter, 220-W, non-magnetically shielded HET called the Western Hall Thruster (WHT44). The RPA consists of an aperture, a series of four parallel grids, and a collection surface. The first grid with respect to a plasma entering the aperture is floating and minimizes the effect of the probe on the surrounding plasma. The second grid is held at a negative potential with respect to facility ground to repel incoming electrons. The third grid acts as the discriminator and is swept from a potential of 0 V to a bias sufficiently above the discharge potential. The fourth grid is held to small negative potential with respect to ground and redirects ion impact secondary electrons formed from the collector surface back to the collector. Following the fourth grid is a solid collection surface held to ground through a picoammeter. For a time averaged RPA, the discriminator grid bias is slowly swept while continuously measuring collector current to obtain the time-averaged RPA current vs. voltage (I-V) profile. At discriminator potentials less than the acceleration potential, the collection current is relatively high because ions have sufficient energy to overcome the electrostatic deceleration fields formed within the RPA. In contrast, when discriminator grid potential is high, relatively few ions can overcome the discriminator potential and very little current is collected. The negative value of the first derivative of current with respect to discrimination voltage yields the ion energy per charge distribution function (IEDF)

$$f(\epsilon) = -dI_{coll}/dV_{bias}. \tag{1}$$

The discriminator voltage is then corrected for the RPA local plasma potential because the bias voltage is measured with respect to facility ground.

B. High-Speed Retarding Potential Analyzer and Temporal Reconstruction

To achieve time-resolved IEDF measurements, one must produce a complete I-V trace at or above the Nyquist cutoff frequency of the plasma oscillation period of interest. Quickly sweeping the bias voltage at a sufficiently high rate to capture I-V traces is one method considered for this study. However, the target application for this diagnostic is to determine the IEDF in the plume of HETs operating from 300 to 600 V and commercially available wideband power amplifiers exceeding 400 V were not readily available. Additionally, it was anticipated that sweep frequencies sufficiently high to be capable of capturing the 100 kHz oscillations would introduce plasma instabilities that would have made extracting meaningful results difficult. An alternative approach, used in this study, is to hold the discrimination grid bias constant and record fast measurements of collector current. The natural flaw in this method is that one cannot simultaneously trigger current measurements at every discriminator potential. Therefore, a temporal reconstruction process must be performed in order to predict a single I-V(t) trace using multiple time-varying collector current signals. The Fast Fourier transform (FFT) method (or transfer function method) was utilized in this study for its relative robustness to noise when using very high sample depths. This method was first applied to Hall thruster probing techniques by Lobbia in an effort to obtain spatiotemporal plasma property measurements in the plume of a 600 W HET.[13] The FFT method generates a frequency domain map from some input signal to an output signal (in our case the HET discharge current I_{disch} and RPA collector current I_{coll} respectively). A linear map is generated by the simple division of complex Fourier output coefficients $A_{coll,i}$ by the input coefficients $A_{disch,i}$, where i represents the discriminator grid bias V_i array index. A unique empirical transfer function is generated for each V_i of interest. Each transfer function is multiplied by an arbitrary coefficient set A^*_{disch} (created from I^*_{disch}) to create a set of coefficients $A^*_{coll,i}$ that represent the frequency domain signal for each V_i. An inverse FFT operation is performed on each $A^*_{coll,i}$ to create the AC component of the collector current $I'_{coll,i}$. Added to this is the mean collector current $\bar{I}_{coll}$, and the final current set, $I_{synthcoll,i}$, can be plotted with respect to V_i to obtain the I-V(t). It then becomes a trivial matter to obtain the time-resolved IEDF using Eq. 3. Figure 1 shows an overview of the signal processing method used to obtain the time-resolved IEDF. The resulting IEDF has a temporal resolution matching that

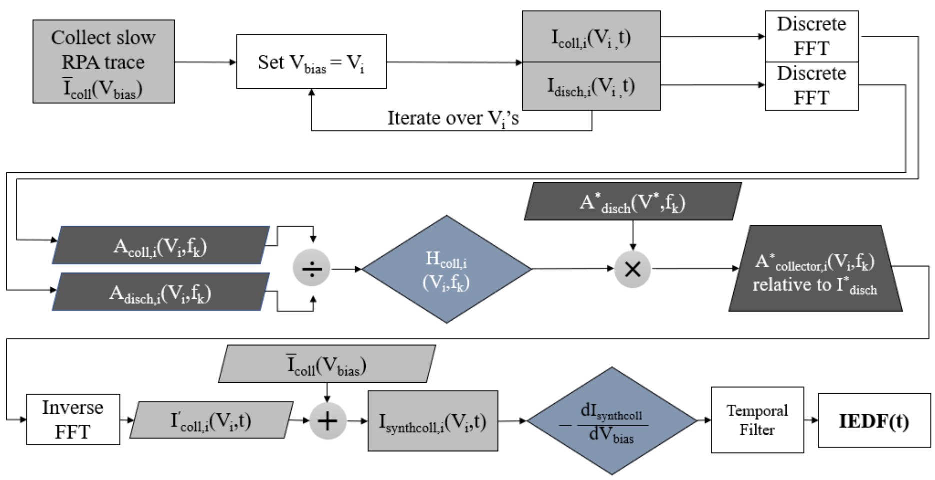

Figure 1: Signal processing flow chart from the raw discharge and collector current signals to a single time-resolved IEDF.

of the original data acquisition sampling frequency and a potential resolution limited by the experimentally collected data. Multi-million or billion point time series data are highly desired for this method. Not only do larger sample sizes increase the signal to noise, but because the frequency resolution obeys

$$\Delta f = \frac{f_s}{N}, \tag{2}$$

where N is the sample depth and f_s is the digitizer sample frequency. The result of larger sample sets is an increased visibility in the low frequency regime and thus a more accurate empirical transfer function.[14]

III. Experimental Setup

Described in this section are the vacuum facility, laboratory thruster, apparatuses, and electronics used to perform the work presented.

A. Facility

Tests were carried out within the 1-m-diameter, 1.5-m-long vacuum chamber located at the Western Michigan University Aerospace Laboratory for Plasma Experiments (ALPE). The facility notionally reaches a base pressure less than 2 μTorr-air using a CTI Cryo-Torr 250F and Turbovac 1100C; however, only the Cryo-Torr pump was used during operation due to electromagnetic noise concerns realted to turbopump operation.

B. Thruster

The low-cost HET testing platform developed at ALPE, herein referred to as the WHT44, was used as the plasma source for the experiment. The WHT44 was designed, fabricated, assembled, and tested with a budget of $2,100 completely in house utilizing common shop and conventional machining equipment (i.e. milling machine, metal lathe, TIG welder, high-temperature oven).[15,16] The WHT was operated at a single operating condition with a discharge voltage of $V_{disch} = 170$ V and a discharge power of $P_{disch} = 240$ W. A 1.6 mm heaterless hollow cathode from Plasma Controls LLC was used to provide electrons for ionization in the thruster and to neutralize the plasma plume. The cathode was placed at 12'o'clock with respect to the floor and positioned such that the keeper emission orifice was within the magnetic sepaeratrix of the WHT44. A cathode flow fraction of 23% was used during this study. This is higher than what is used in typical HET operation and was used in the WHT44 for these experiments to maintain a quiescent thruster discharge and prevent thruster shutdown. The facility pressure remained at 8.9×10^{-4} Torr-Xe for the duration of this experiment. We concede this to be a very high operational pressure; however, this was the lowest pressure achievable for flow rates that resulted in quiescent thruster operation with limited facility pumping capacity. The increase in background pressure likely impacts thruster dynamics due to neutral ingestion and CEX ions, resulting in oscillation dampening. Because the purpose of this study was to test the validity of the diagnostic on an HET and not obtaining true flight-like thruster energy distributions, this was deemed acceptable. Common programmable laboratory power supplies were used to power the cathode keeper, thruster discharge, and series magnets. The thruster body was tied to cathode and allowed to float with respect to vacuum facility ground. The WHT44 can be seen operating at a discharge power of 240 W in Fig. 2.

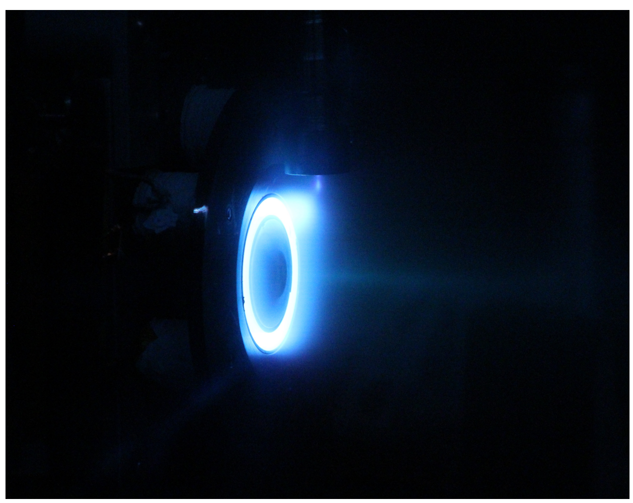

Figure 2: Photograph of the WHT44 operating at a discharge power of 240 W.

C. Retarding Potential Analyzer Probe and Instrumentation

An RPA was designed, fabricated, and validated in support of this experiment. The RPA body, grids, retention rings, and wires were made from 316 stainless steel. Alumina tubing 1.6 mm in diameter was used to insulate the grid wires and MACOR was used as an insulator between grids and between the grid stack and the RPA body. A grid assembly was formed by spot welding a wire mesh grid to a metal ring, then spot welding a wire to the ring, and finally, slipping alumina tubing over the wire of an appropriate length. Figure 3 shows the grid and insulator geometry of the RPA used in this experiment. A non-uniform grid configuration was selected to avoid Moire patterns of variable transparency across the grid. The geometric details of each grid as well as an example spot welded grid assembly are also shown in Fig. 3.

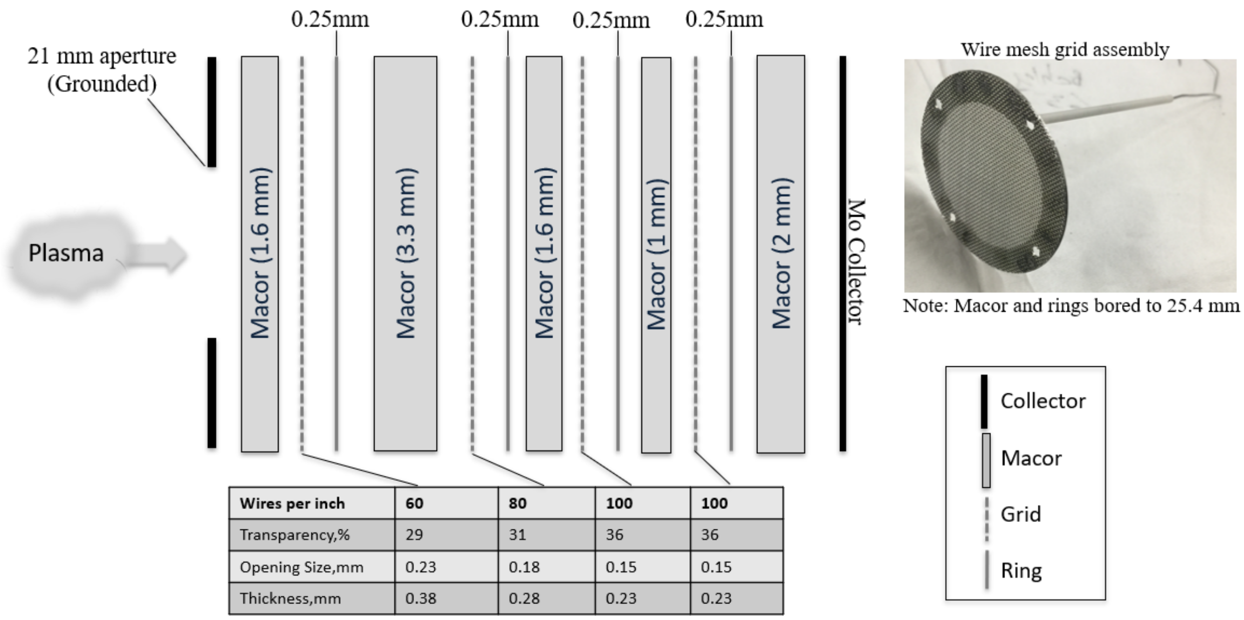

Wires per inch	60	80	100	100
Transparency,%	29	31	36	36
Opening Size,mm	0.23	0.18	0.15	0.15
Thickness,mm	0.38	0.28	0.23	0.23

Figure 3: Illustration showing the RPA grid and insulator arrangement. The lower table shows the individual grid properties and legend to the lower right identifies the RPA internal components.

The electron repulsion grid was held to -58 V, and the electron suppression grid to -19 V with series banked standard 9 V batteries and referenced to facility ground. These grid setpoints were found through iteration and produced acceptable I-V traces during an RPA operational verification test with a 1 cm Kaufman & Robinson, Inc. gridded ion source. The RPA was demonstrated at beam voltage levels ranging from 100 V to 800 V in 50 V increments. The normalized results of the ion source validation experiment, uncorrected for plasma potential, showed highly correlated IEDF peak to beam voltage behavior as shown in Fig. 4.

In order to temporally reconstruct the IEDF, collector currents below a microampere were required to be collected at frequencies exceeding the dominant thruster oscillatory mode. To achieve this, a custom 1 MHz 10^6 V/A transimpedance amplifier (TIA) was connected to the RPA collection surface. A mechanical relay allowing the collector current to be quickly bypassed to a Keithley 487 picoammeter for time-averaged I-V traces was located at the TIA input. The grids and insulators were housed inside the RPA body which was held to facility ground potential to minimize collector current noise. With the exception of battery conductors, only shielded cables were used.

The TIA was mounted as close to the facility feedthrough as practical to minimize destabilizing input capacitance. The RPA was mounted off-thruster-centerline by $\theta = 35.5°$ and at a radial distance of $R = 468$ mm. This position enabled the measurement of both slow and fast ion populations. During WHT44 testing, electron repulsion and suppression grid bias voltages were set to the same values as the ion source validation experiment, and discriminator bias voltage ranged from 0 V to 300 V in 10 V increments. Around V_{disch}, between 140 V and 200 V, the discriminator voltage increment was decreased to 5 V. A simplified diagram illustrating the diagnostic and relative location with respect to the WHT44 is shown in Fig. 5.

A non-uniform V_{bias}, 37-energy level testing matrix was selected on the basis of giving a slight boost in energy resolution near the thruster discharge voltage.

$$V_{bias,i} = [0 : 10 : 140, 145 : 5 : 200, 210 : 10 : 300]V. \tag{3}$$

A sample depth of 50 million samples was used during this experiment; although, it should be mentioned that the FFT analysis methods used in this paper would likely benefit from the full digitization sample depth of 1 billion samples. Two channel data collection (I_{disch} & I_{coll}) at a sample collection frequency of 50 MHz for 1 second saved as a raw binary file yields over 0.5 gigabytes of data for each V_{bias} setpoint. Upon completion of data collection, roughly 18.8 gigabytes of data were collected. While temporal reconstruction

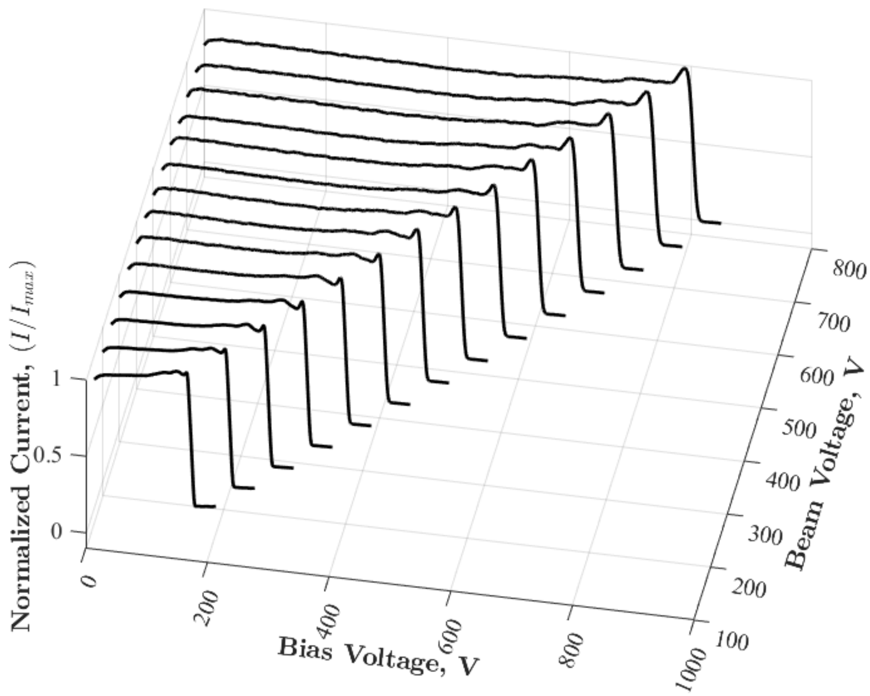

Figure 4: RPA validation results obtained with a 1 cm Kaufman & Robinson, Inc. gridded ion source. Beam voltages between 100 V and 800 V were tested in 50 V increments. The I-V traces have been normalized to the maximum collector current for each trace.

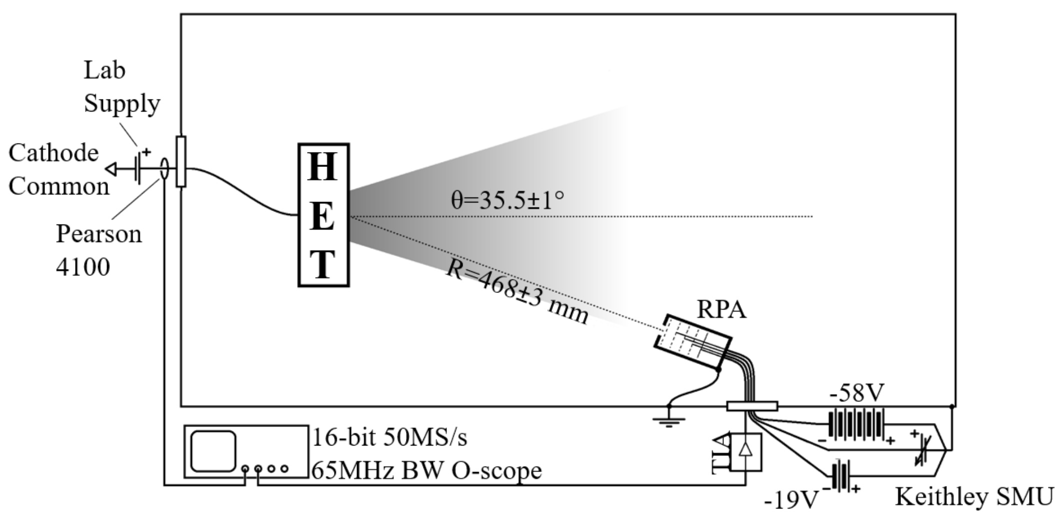

Figure 5: Diagram showing the experimental setup.

would have likely benefited from a larger sample depth or higher energy resolution, a balance between data volume (and thus, post-processing computational time) and energy resolution was necessary.

IV. Experimental Results

The first metric used to determine the accuracy of the diagnostic is a comparison between the slowly swept RPA trace and time series statistics at each V_{bias}. This simple comparison demonstrates the DC accuracy of the TIA and the noise floor of the analysis. The slowly swept Keithley 487 RPA results are shown as a grey dashed line, the mean of the 50 MHz data is shown as a hollow point, half the peak to peak value is shown as a thin error bar, and the standard deviation is shown as a thick error bar in Fig. 6. Figure 6 also shows the slow speed dI_{coll}/dV_{bias} as a blue dashed line. The IEDF below a 15 V bias was

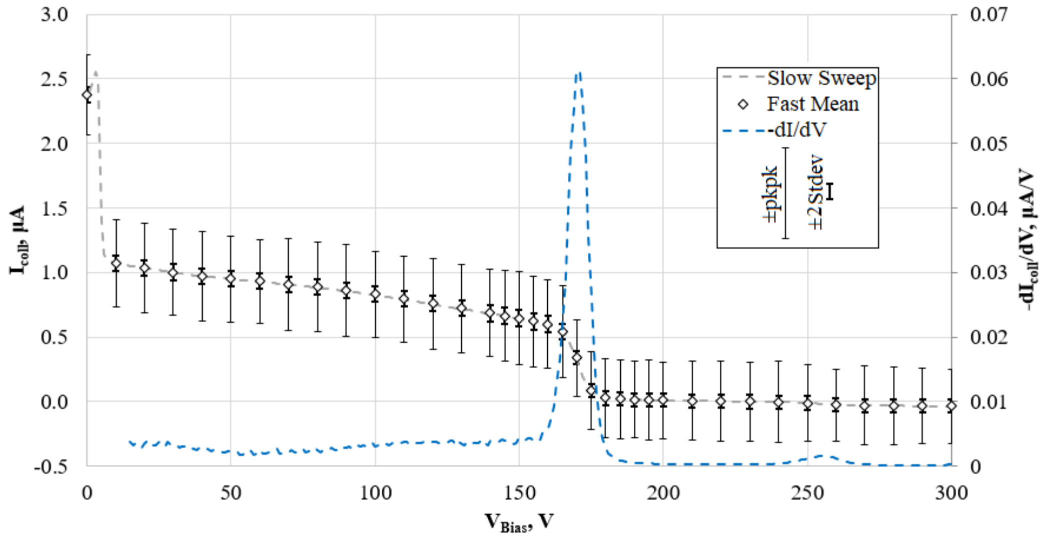

Figure 6: Slow RPA sweep (grey dashed line) plotted alongside the mean, peak to peak, and standard deviation of the 50 MHz data over 50 million samples (black symbols). The slowly swept first differential is plotted in a blue dashed line. The first 15 points of the differential are omitted for clarity.

excluded for clarity. The main beam ions are clearly present near 170 V and below 170 V a broad lower energy population is present. A small distribution of ions are measured near a bias voltage of 250 V. These ions are measured at energies nearly 100 V greater than the HET acceleration potential.

The mean discharge current FFT is shown in Fig. 7 left. This illustrates the average spectral density of the thruster while operating over the course of the entire experiment. An FFT analysis was performed on the raw I_{coll} signal at each V_{bias} tested and is shown in Fig. 7 right. Figure 7 was used to compare the spectral content of the thruster discharge to the spectral content filtered by the RPA.

The temporal reconstruction process described earlier in this paper was applied to these data, and the IEDF as a function of bias voltage and time is shown in Fig. 8.

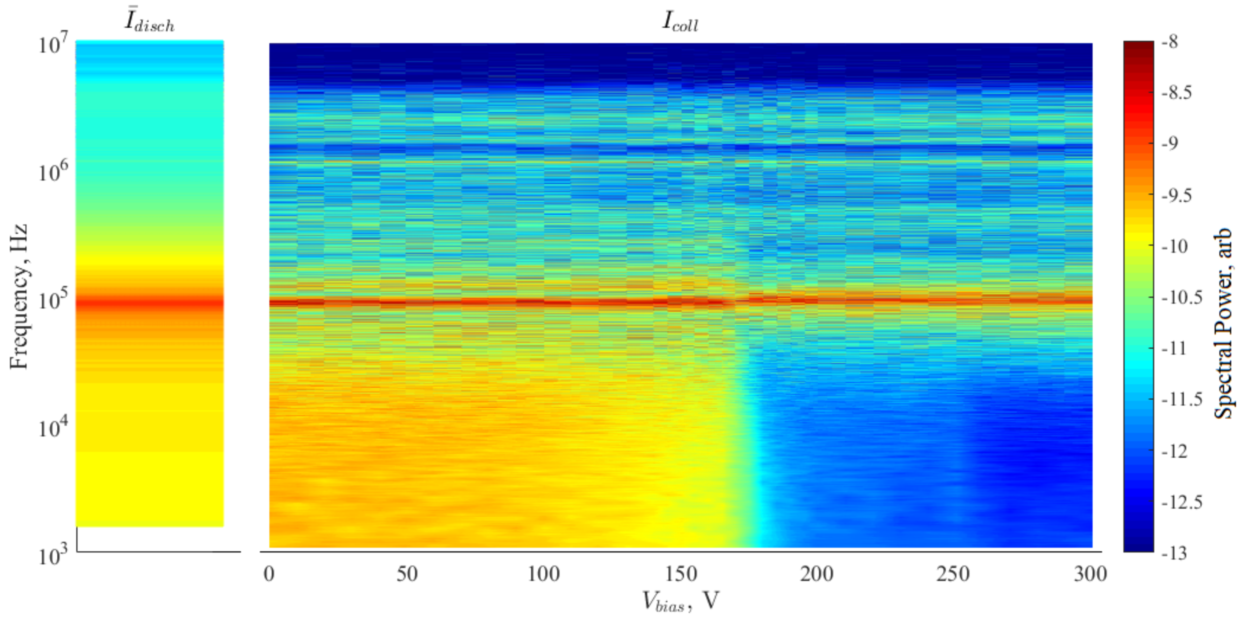

Figure 7: Discharge current spectral power density average over all high speed data (left) and collector current spectral power density as a function of discriminator grid bias (right).

V. Discussion

The I_{coll} spectral power decreases sharply at a V_{bias} equal to that of the thruster discharge potential. This is especially apparent at lower frequencies but is observable at frequencies as high as 280 kHz. This is probably in large part due to the absence of spectral content of the thruster discharge current above 280 kHz. Spectral energy change as a function of V_{bias} suggests that there are frequencies that are specific to certain ion energy populations. The persistent horizontal line at 91 kHz is coupled to the dominate thruster oscillation mode. It is noticeable that this oscillation is still present at even the highest V_{bias}; however, theoretically, it should have been filtered out. Substantial care was taken to shield the RPA and harnessing from the plasma and other sources of electromagnetic interference, so the exact mechanism behind this effect is unknown. The 91 kHz spectral power invariance to V_{bias} could be suggestive of noise coupling to the collector rather than a physical measurement of ion population oscillations (e.g. a capacitively coupled displacement current between the effectively grounded collector and surrounding plasma). However, we do not completely dismiss that this phenomenon is real. Additional observations from Fig. 7 include:

- The spectral "drop off" does not all occur at the same V_{bias}, rather it occurs non-uniformly which may suggest the higher energy ion oscillations are correlated with a slightly lower oscillation frequency.
- The spectral power roll off from 0 to 170 V occurs gradually, which is the same trend witnessed in the time-averaged I-V trace of Fig. 6.
- There is a secondary uniform decline of spectral density at 250 V. This trends with a small secondary decrease in collected current at 250 V in the time averaged trace shown in Fig. 6.

High-energy ions above the potential differences associated with hollow cathodes have been observed in prior investigation of high current hollow cathodes.[17,10] A plausible source of the high-energy ions in this study could be the hollow cathode. However, the cathode current in this study was relatively low at less than 1.5 A and warrants additional investigation.

It was originally hypothesized that a heavy coupling between the main ion beam energy distribution oscillations and the thruster discharge current would exist. However, the first observation from Fig. 8 is only mild coupling between the thruster discharge and the 170 V beam ion distribution. Again there is an apparent steady high ion energy population at 250 V. A complex low-energy ion population is visible at sub-170 V energy levels. Due to the high operating pressures, it is unlikely that these low-energy ions

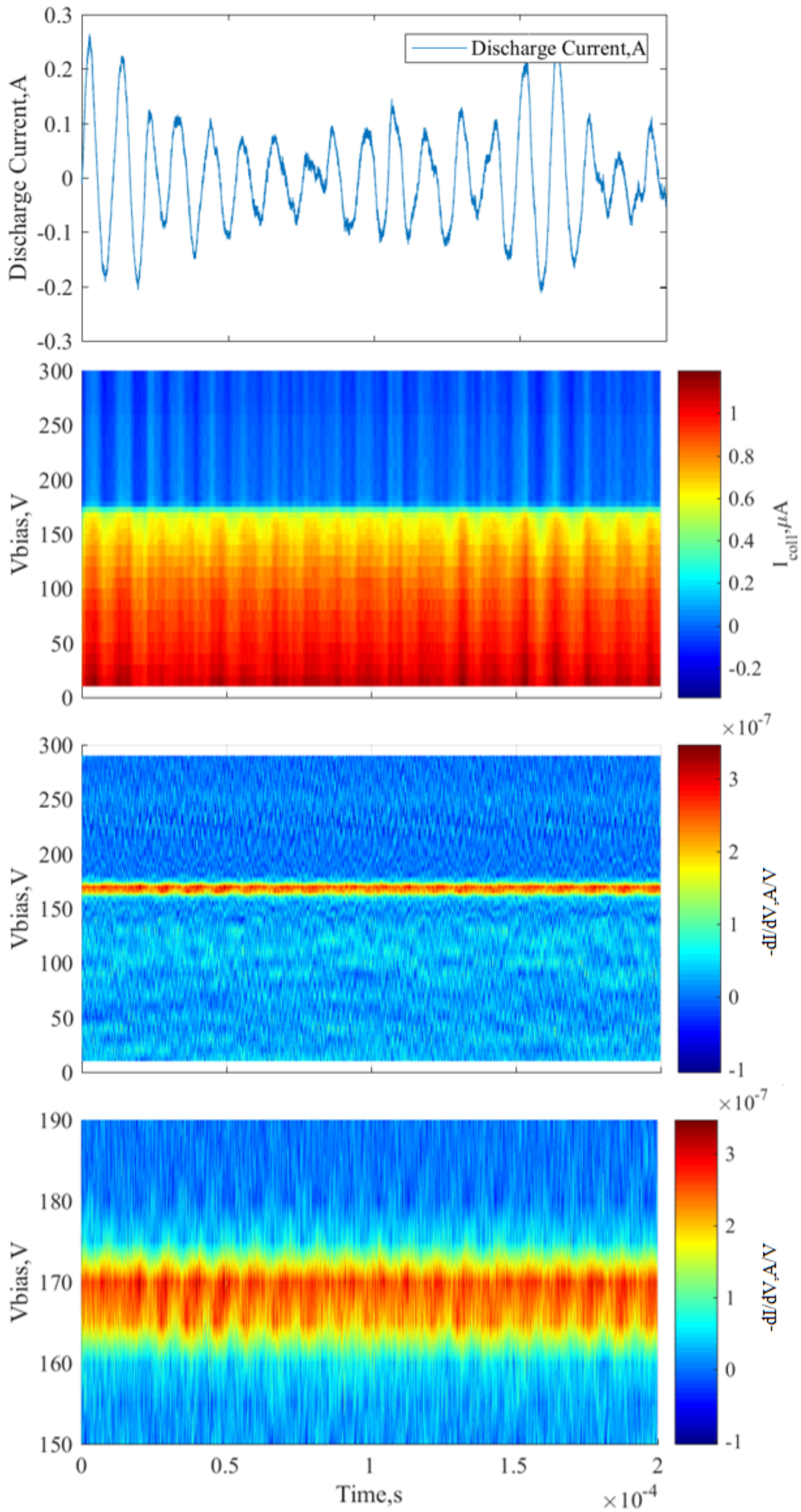

Figure 8: Thruster discharge current sampled over 100 μs (first), the associated I-V(t) (second), the associated temporally reconstructed IEDF (third), and a zoomed view of the IEDF(t) about the thruster discharge voltage (fourth).

measured within the ambient plasma are representative of the true IEDF sourced directly from the thruster, and are likely the result of complex CEX and wave dampening.

A notable benefit to the methods proposed in this paper is that the reconstructed temporal resolution matches that of the data acquisition sampling rate. However, the final IEDF time series data were filtered using a Matlab 1^{st} order sgolayfilt() smoothing function. As mentioned, previously, a sample depth of 50 million samples was used for this experiment, and the method would have likely benefited from a reduction in noise from sample depths an order of magnitude greater. Likewise, an increased bias resolution about the V_{disch} was manually selected for reasons of practical data management and experimental duration; however, future studies may benefit from automated data collection and an increased discriminator bias density.

A drawback to the analysis techniques is the rather cavalier treatment of ion transit time within the RPA. An initial assumption was made that the ion transit time Δt is unperturbed by electric fields within the RPA (i.e. $\Delta t = dv_0$, where d is the characteristic axial length of the RPA grid assembly and v_0 is the ion entry velocity). The limits of this assumption become apparent when performing a piece-wise second integration of the axial magnetic field-free Lorentz force equation over each grid segment,

$$m\frac{d^2z}{dt^2} = qE_z. \tag{4}$$

Assuming that ions enter each grid with the same kinetic energy with which they left the previous grid, it can be seen that the transit time through the RPA may be significantly different from that of an unperturbed ion traveling the same distance. This reveals the simple fact that ion transit times within the RPA are non-linear with respect to energy. For the geometry, ion transit times within the RPA form a non-linear relationship of ion energy population and filtration energy that introduce errors in the measurement, such as phase lag, that are not accounted for in this proceeding. This work represents the first step in exploring the viability of this analysis. More thorough analysis planned in future work may correct for errors related to ion transit time and thus provide a more accurate discharge current coupled IEDF.

Other methods for temporal reconstruction, such as shadow manifold interpolation (SMI), have recently been made applicable to Hall thruster testing.[18] The SMI method shows good potential and was considered and deferred to later work.

VI. Conclusion

A method for measuring the time-resolved IEDF was presented. The method utilizes an FFT based temporal reconstruction technique previously utilized in high-speed Langmuir probe measurements and high-speed laser induced fluorescence. This work was able to provide visibility to the complex temporal ion behavior in the sub-discharge voltage energy regime in the plume of a non-magnetically shielded HET.

Acknowledgments

This work was supported by a NASA Space Technology Research Fellowship grant number NNX16AM96H. The authors would also like to thank Ron Fitzgerald McGee-Sinclair for his efforts in preparing the facilities, which enabled timely completion of the presented experiments.

References

[1] Dan M. Goebel and Ira Katz. *Fundamentals of Electric Propulsion: Ion and Hall Thrusters*. Hoboken, NJ: John Wiley & Sons, Inc., 2008. ISBN: 9780470429273. DOI: 10.1002/9780470436448. URL: https://descanso.jpl.nasa.gov/SciTechBook/series1/Goebel{_}{_}cmprsd{_}opt.pdf.

[2] David Y Oh et al. "Development of the Psyche Mission for NASA's Discovery Program". In: *35th Int. Electr. Propuls. Conf.* Atlanta, GA, 2017. URL: http://erps.spacegrant.org/IEPC{_}2017/IEPC{_}2017{_}153.pdf.

[3] David Y Oh et al. "Psyche: Journey to a Metal World". In: *52nd AIAA/SAE/ASEE Jt. Propuls. Conf.* Salt Lake City, UT, 2016. DOI: 10.2514/6.2016-4541. URL: http://arc.aiaa.org.

[4] Michelle Rucker and John Connolly. *Deep Space Gateway-Enabling Missions to Mars*. Tech. rep. 2017. URL: https://ntrs.nasa.gov/search.jsp?R=20180000122.

[5] Jason D. Frieman et al. "Long Duration Wear Test of the NASA HERMeS Hall Thruster". In: *54th AIAA/ASME/SAE/ASEE Jt. Propuls. Conf.* Cincinatti, OH, 2018. ISBN: 978-1-62410-570-8. DOI: 10.2514/6.2018-4645. URL: http://arc.aiaa.org.

[6] Richard R. Hofer et al. "Development Status of the 12.5 kW Hall Effect Rocket with Magnetic Shielding (HERMeS)". In: *53th AIAA/ASME/SAE/ASEE Jt. Propuls. Conf.* Atlanta, GA, 2017. URL: https://iepc2017.org/sites/default/files/speaker-papers/iepc-2017-231{_}hofer{_}r02.pdfhttp://erps.spacegrant.org/IEPC{_}2017/IEPC{_}2017{_}231.pdf.

[7] Wensheng Huang, Hani Kamhawi, and Thomas W. Haag. "Plasma Oscillation Characterization of NASA's HERMeS Hall Thruster via High Speed Imaging". In: *52nd AIAA/SAE/ASEE Jt. Propuls. Conf.* Salt Lake City, UT, 2016. DOI: 10.2514/6.2016-4829. URL: http://arc.aiaa.org.

[8] Benjamin A. Jorns and Richard R. Hofer. "Plasma oscillations in a 6-kW magnetically shielded Hall thruster". In: *Phys. Plasmas* 21.5 (2014), p. 053512. ISSN: 1070-664X. DOI: 10.1063/1.4879819. URL: http://aip.scitation.org/doi/10.1063/1.4879819.

[9] Michael J. Sekerak. "Plasma Oscillations and Operational Modes in Hall Effect Thrusters". PhD thesis. Plasma Oscillations and OperationaModes in Hall Effect Thrusters, 2014. URL: http://pepl.engin.umich.edu/pdf/2014{_}Sekerak{_}Thesis.pdf.

[10] Ikuya Kameyama and Paul J. Wilbur. "Measurements of Ions from High-Current Hollow Cathodes Using Electrostatic Energy Analyzer". In: *J. Propuls. Power* 16.3 (2000). URL: https://arc-aiaa-org.libproxy.library.wmich.edu/doi/pdf/10.2514/2.5601.

[11] Christopher J. Durot et al. "Laser-Induced Fluorescence Measurement of the Anomalous Collision Frequency in a 9-kW Magnetically-Shielded Hall Thruster". In: *35th Int. Electr. Propuls. Conf.* Atlanta, GA, 2017. URL: http://erps.spacegrant.org/IEPC{_}2017/IEPC{_}2017{_}29.pdf.

[12] Marcel P Georgin et al. "Passive High-speed Imaging of Ion Acoustic Turbulence in a Hollow Cathode". In: *53nd AIAA/SAE/ASEE Jt. Propuls. Conf.* Atlanta, GA, 2017. DOI: 10.2514/6.2017-4973. URL: http://arc.aiaa.org.

[13] Robert B. Lobbia and Brian E. Beal. "Recommended Practice for Use of Langmuir Probes in Electric Propulsion Testing". In: *J. Propuls. Power* (2016), pp. 1–24. ISSN: 0748-4658. DOI: 10.2514/1.B35697. URL: http://arc.aiaa.org/doi/10.2514/1.B35697.

[14] Robert B. Lobbia. "A Time-resolved Investigation of the Hall Thruster Breathing Mode". PhD thesis. University of Michigan, 2010. URL: http://pepl.engin.umich.edu/pdf/2010{_}Lobbia{_}Thesis.pdf.

[15] Matthew J. Baird, Nagual A. Simmons, and Kristina M. Lemmer. "Design and Initial Operation of a Small Low-cost Hall Thruster". In: *35th Int. Electr. Propuls. Conf.* Atlanta, GA, 2017. URL: http://erps.spacegrant.org/IEPC{_}2017/IEPC{_}2017{_}534.pdf.

[16] Matthew J. Baird, Nagual A. Simmons, and Kristina M. Lemmer. "Performance characterization of a small low-cost Hall thruster". In: *35th Int. Electr. Propuls. Conf.* Atlanta, GA, 2017. URL: http://erps.spacegrant.org/IEPC{_}2017/IEPC{_}2017{_}535.pdf.

[17] Verlin J Friedly and Paul J Wilburt. "High Current Hollow Cathode Phenomena". In: *J. Propuls. Power* 8.3 (1992), pp. 635–643. DOI: 10.2514/3.23526. URL: http://arc.aiaa.org.

[18] Daniel Eckhardt et al. "Spatiotemporal data fusion and manifold reconstruction in Hall thrusters". In: *Plasma Sources Sci. Technol* Not yet pu (2019).